Applied Catalysis B: Environmental 337 (2023) 122927

Contents lists available at ScienceDirect

Applied Catalysis B: Environmental

journal homepage: www.elsevier.com/locate/apcatb

Order-of-magnitude increase in rate of methane dry reforming over Ni/CeO_2-SiC catalysts by microwave catalysis

Yu Shi [a], Lei Wang [a], Mengmeng Wu [b], Fagen Wang [a,b,*]

[a] School of Chemistry and Chemical Engineering, Jiangsu University, Zhenjiang 212013, PR China
[b] State Key Laboratory of Clean and Efficient Coal Utilization, Taiyuan University of Technology, Taiyuan 030024, Shanxi, PR China

ARTICLE INFO

Keywords:
Microwave catalysis
Ni/CeO_2-SiC catalyst
Low carbon
Methane dry reforming

ABSTRACT

Methane dry reforming (MDR) produces syngas from CH_4 and CO_2. The endothermic character of the reaction forces the lower surface catalyst temperature than targeted furnace temperature in thermal catalysis, which decreases carbon gasification ability and prones to deactivate catalyst. Increasing catalyst surface temperature is a way to enhance the gasification ability. In this work, we designed Ni/CeO_2-SiC catalysts for MDR under microwave irradiation. The microwave adsorption by Ni and SiC increased the surface temperature of catalyst, significantly enhancing MDR performance and considerably reducing carbon deposition compared with those in thermal catalysis. CH_4 and CO_2 rates reached 16.5 mmol/(g_{Ni}·s) and 18.6 mmol/(g_{Ni} s), respectively, on the 1Ni/CeO_2-SiC. The rates were one order-of-magnitude increased when be compared in literatures. Carbon deposits were as 1.4 wt% by microwave catalysis in comparison to 5.0 wt% by thermal catalysis on the used 1Ni/CeO_2-SiC catalyst. The work explores a more effective microwave catalysis of Ni/CeO_2-SiC catalyst for high-performance MDR.

1. Introduction

The fossil fuels consumption emits huge greenhouse gases to the atmosphere, leading to serious problem of global warming. Methane dry reforming (MDR) converts greenhouse gases of CH_4 and CO_2 to syngas, which is valuable for Fischer-Tropsch and carboxylation to produce energy chemicals. It is thus greatly paid attention on in decades reducing the greenhouse gases and producing renewable energies [1–5]. In traditional thermal catalysis, catalyst is heated by electric furnace. The endothermic property of MDR ($CH_4 + CO_2 \rightarrow 2CO + 2\,H_2$, $\triangle H_{298} = +247$ kJ/mol) and the loss of heat when it transfers from furnace to catalyst bed make the lower catalyst surface temperature than the targeted temperature. This causes the lower performance and the weaker carbon gasification ability, which prones to deactivate catalyst [6,7]. Microwave irradiation is another way to heat catalyst when the catalyst can adsorb microwave, which has faster heating rate, less heating loss and higher energy efficiency. The adsorbed microwave energy is transformed to heat energy, giving increased temperature on catalyst surface.

Since R. Giguere et al. employed microwave to synthesis organic chemicals [8], the microwave technique has been extensively applied in other domains including MDR [9,10]. B. Fidalgo et al. used activated carbon as microwave receptor, the higher CH_4/CO_2 conversions were obtained by microwave heating than by conventional electronic furnace heating, the effect of microplasmas (local hot heating) was ascribed to the better performance [11]. H. M. Nguyen et al. were the first researchers studying microwave catalysis of MDR over metal-based catalysts, they found that Co or Mo monometallic catalyst was inactive while Co-Mo bimetallic catalyst displayed MDR activity, which was because that Co and Mo couldn't absorb microwave due to their low magnetic properties, while the magnetodielectric CoMo alloy was good at adsorb microwave [12]. Therefore, microwave irradiation is another way to heat catalyst when the catalyst can adsorb microwave, which has advantageous of faster heating rate, less heating loss and higher energy efficiency. The adsorbed microwave energy is transformed to heat energy, giving increased temperature on catalyst surface and improving catalytic performances [9,10].

Ni nanoparticle is the active metal that can strongly adsorb microwave and actively catalyze MDR, while SiC is the support that can strongly adsorb microwave and effectively transform the adsorbed microwave to heat [13,14]. The transformation of microwave to heat increases the surface temperatures of Ni and SiC, therefore the catalyst composing Ni and SiC shall more active to MDR by microwave catalysis

* Corresponding author at: School of Chemistry and Chemical Engineering, Jiangsu University, Zhenjiang 212013, PR China.
E-mail address: fagen.wang@gmail.com (F. Wang).

https://doi.org/10.1016/j.apcatb.2023.122927
Received 24 March 2023; Received in revised form 12 May 2023; Accepted 28 May 2023
Available online 30 May 2023

than by traditional thermal catalysis, showing lower carbon deposition and stronger stability [9]. Z. Zhang et al. applied Ni-La_2O_3/SiC catalysts for DRM, the higher Ni-sintering resistance by strong Ni-La_2O_3 interaction and the rapid heat transfer by high thermal conductivity of SiC contributed to the much enhanced coke-depositing/Ni-sintering resistances of Ni-La_2O_3/SiC than Ni-La_2O_3/Al_2O_3 [15]. R. Li et al. reported Ni-Co/ZrO_2-CaO catalyst mixed with SiC for MDR, CH_4 and CO_2 conversions were up to 97.1 % and 99.2 %, respectively, at 1273 K by microwave catalysis, much higher than those of 75.7 % and 82 % by traditional thermal catalysis. The accelerated elimination of carbon gasification and the reduction of apparent activation energy by microwave were assigned to the lower carbon deposition and the higher performance [16]. I. Garcia et al. pointed that Ni/Al_2O_3 could not adsorb microwave, but the required temperature could be reached when it was mixed with SiC. CH_4 and CO_2 conversions were 90 % over the Ni/Al_2O_3-SiC under microwave irradiation, in comparison to 79 % under furnace heating at 1273 K [17]. Some researchers use SiC as foam to support Ni catalysts, by which cellular open-cell structure of the foam intensified transportation compared to traditional packed bed, giving higher MDR activity and stability [18,19].

Although the achievements obtained above, some shortages are hard to be overcame in microwave catalysis. In order to pursue considerable conversions of CH_4 and CO_2, high power is always input. However, the high input power would make the large energy consumption and the easy Ni sintering [17]. This is because that the high input power always leads to the higher temperature on catalyst, the immigration of Ni is more favored and thus aggregation is faster in microwave catalysis than in traditional thermal catalysis. The severe aggregation results in consequences of Ni nanoparticles sintering and carbon deposits accumulation, which would decay MDR performance. For example, H.M. Nguyen et al. performed MDR reaction using microwave power from 200 W to1000 W, in which MDR performance could be maintained under input of 200 W, while the performance was minorly declined under 500 W and was apparently decayed under 1000 W [12]. Aiming to resolve the shortages, we innovatively designed Ni/CeO_2-SiC catalysts for MDR by using CeO_2 to enhance metal-support interaction and by applying SiC to adsorb microwave in a microwave fixed-bed reactor (Fig. S1). The input of power was downed to 200 or 300 W. The experimental results showed that size of Ni nanoparticles was marginally changed and carbon deposition was greatly lessened by microwave catalysis, obtaining higher strengthened stability. The rates of CH_4 and CO_2 were one order-of-magnitude increased by microwave catalysis compared with pioneers' results, showing great advantages of microwave catalysis for MDR over the Ni/CeO_2-SiC catalysts.

2. Experimental

2.1. Catalyst preparation

0.6 g $CO(NH_2)_2$ and 1.0 g SiC powders were dissolved in 60 mL deionized water, $Ni(NO_3)_2$ and $Ce(NO_3)_3$ aqueous solutions were dropped to the SiC suspension (mass fraction of CeO_2 was 5.0 wt%, and Ni mass ratio was adjusted to 1.0 wt%, 3.0 wt% and 5.0 wt%). After stirring at 298 K for 1 h, the mixture was sealed into a Teflon-lined autoclave for heating at 443 K for 12 h. The final precipitate was filtrated and collected by centrifugation and the obtained slurry was washed by deionized water 3 times. The resultant production was dried at 333 K overnight and was calcined at 773 K for 4 h obtaining powders of xNi/CeO_2-SiC catalysts (x = 1, 3 and 5). Following the same procedures, Ni/CeO_2-SiC catalysts with Ni loadings of 10 wt%, 15 wt% and 20 wt% and with CeO_2 loadings of 0 wt%, 10 wt%, 15 wt% and 20 wt% were also prepared.

2.2. Catalyst characterization

The actual Ni contents of the catalysts were measured by inductively coupled plasma atomic absorption spectrometry (ICP). Brunauer-Emmett-Teller (BET) surface areas and Barrett-Joyner-Halenda (BJH) pore distributions were measured by surface analyzer (Tristar II 3020, Micromeritics) at 77 K after catalyst degassing. X-ray power diffraction (XRD) patterns were recorded by an X-ray diffractor (XRD-6100X, Shimadzu) running at 40 kV and 30 A. Morphologies of the catalysts were characterized on JEOL 2010 transmission electron microscopy (TEM) at 200 kV. Raman was measured in a Laser Micro Raman Spectrometer (Thermal Scientific DXR) using 532 nm laser as excitation source. Thermogravimetry (TG) was performed by thermogravimetric analyzer (SDTQ 600) in air atmosphere at rate of 10 K/min. H_2 temperature-programmed reduction (H_2-TPR) of fresh catalysts was performed by an H_2-chemisorption analyzer (AutoChem II 2920) referencing [20]. H_2 temperature-programmed desorption (H_2-TPD) experiment was carried on after the previous H_2-TPR experiment. Once the reduction was done, the sample was cooled to room temperature in the flow of 5 %H_2/N_2 gas mixture. The adsorption of H_2 was lasted for 2 h, then Ar was purged for 2 h to remove physical adsorbed H_2 and to stabilize TCD detector. The sample was then heated to 1023 K for 30 min and the signal was monitored by the TCD detector.

Electromagnetic adsorption was evaluated using a vector network analyzer (Agilent N5234A) at frequency of 2–18 GHz. The reduced 3Ni/CeO_2-SiC sample powders (with size less than100 mesh) were mixed with paraffin and extruded into a ring-shaped test ring with ϕ_{out} of 7.00 mm, ϕ_{in} of 3.04 mm and ϕ_{height} of 2.00 mm. The weight percentages of the sample were from 30 % to 50 %.

The parameters of permittivity and permeability were tested and the reflection loss (RL) and impedance of microwave absorption are based on: [21]

$$\mathrm{RL(dB)} = 20\log\left|\frac{Z_{in} - Z_0}{Z_{in} + Z_0}\right| \tag{1}$$

$$Z_{in} = Z_0\sqrt{\frac{\mu_r}{\varepsilon_r}}\tanh\left(j\frac{2\pi fd}{c}\right)\sqrt{\mu_r\varepsilon_r} \tag{2}$$

where Z_0 is the impedance of the free space, Z_{in} is the normalized input impedance, ε_r and μ_r are the relative complex permittivity and permeability, f is the microwave frequency, d is the thickness of the absorber, and c is the velocity of light.

The dielectric and magnetic loss tangents are according to: [22].

$$\tan\delta_\varepsilon = \frac{\varepsilon''}{\varepsilon'} \tag{3}$$

$$\tan\delta_\mu = \frac{\mu''}{\mu'} \tag{4}$$

where μ' and ε′ are real parts of permeability and permittivity, respectively, and μ'' and ε″ are imaginary part of permeability and permittivity, respectively, for the dissipative capacity of microwave. The values of ε′ and ε″ can be expressed as: [23]

$$\varepsilon' = \varepsilon_\infty + \frac{\varepsilon_s - \varepsilon_\infty}{1 + (2\pi f\tau)^2} \tag{5}$$

$$\varepsilon'' = \frac{2\pi f\tau(\varepsilon_s - \varepsilon_\infty)}{1 + (2\pi f\tau)^2} \tag{6}$$

where ε_s is the static dielectric constant, ε_∞ is the relative dielectric constant at the high frequency limit, f is the frequency, and τ is the polarization relaxation time.

2.3. Energy efficiency of thermal and microwave catalysis of MDR

The energy efficiency analysis here is based on the macroscopic energy balance, which can be expressed as:

$$\sum_i n_{i,in}\int_{T_0}^{T_p} C_{p_i}(T)dT - \sum_i n_{i,out}\int_{T_0}^{T_{out}} C_{p_i}(T)dT - \Delta H_r^{T_0} + Q_{input} - Q_{loss} = 0 \quad (7)$$

n_i is the mole number of species i; T_0 is the ambient temperature; T_p is the temperature of preheated reactants entering the catalytic bed; T_{out} is the temperature of the products at the outlet; Q_{input} is the energy delivered to the bed either from the electric heating element or from the magnetron (i.e., electromagnetic energy dissipated in the bed), and Q_{loss} is the heat loss through the solid boundaries.

The above equation can be rewritten as:

$$\sum_i n_{i,in}\int_{T_0}^{T_p} C_{p_i}(T)dT + Q_{input} - Q_{loss} = \Delta H_r^{T_0} + \sum_i n_{i,out}\int_{T_0}^{T_{out}} C_{p_i}(T)dT \quad (8)$$

In the equation, the left side means the net energy input for the reaction including preheating reactants, the heat input and the heat loss; while the right side means that the net heat input is partially converted to chemical energy and partially leaves the system as heat of the products On this basis, T. Durka et al. define energy efficiency as the fraction of net heat input converted to chemical energy, expressing as: [24]

$$\omega = \frac{\Delta H_r^{T_0}}{\Delta H_r^{T_0} + \sum_i n_{i,out}\int_{T_0}^{T_{out}} C_{p_i}(T)dT} * 100\% \quad (9)$$

2.4. MDR catalytic performance test

MDR was conducted on a microwave fixed-bed reactor. The configuration image of the reactor and the microwave cavity with detailed dimensions are given in Fig. S1. The power of the microwave fixed reactor can be automatically tuned between 200 W and 300 W to heat the catalyst or keep the catalyst at a designed temperature. The electromagnetic wave is provided by a magnetron with wave mode of multimode. An iron hollow column with diameter of 10 mm is positioned in the reactor for hosting quartz reactor, in which catalyst powders are loaded. In order to minimize the inhomogeneous temperature distribution in the catalyst bed as much as possible [25], the catalysts were seized to powders with size less than 100 mesh, and the height of catalyst bed was less than 5 mm. The temperature of the reactor is monitored by K-type thermocouple attaching in the middle of the iron column, and the temperature of catalyst bed is measured by optical fiber probe.

50 mg catalyst was loaded in a quartz tube and was heated to 1023 K in the 25 %H_2/N_2 flow within 30 min by microwave irradiation (200 W). The reduction was lasted for 1 h at 1023 K. Then the mixture of $CH_4/CO_2/N_2$ (molar ratio 3/3/4, 50 mL/min) was introduced and the MDR activity was measured starting from targeted temperature of 1023 K. The temperature was naturally decreased at the interval of 50 K for temperature-dependent activity measurements. At each temperature, the MDR reaction was conducted for 30 min to achieve the steady state. As a comparison, traditional thermal MDR was carried using electric furnace to provide temperature. Outlet gases were analyzed by TCD in online gas chromatography. CH_4 and CO_2 conversions, rates, H_2/CO ratio and carbon balance were calculated by the formula below.

$$\text{Conversion}: X_i = (1 - F_{i,outlet}/F_{i,inlet}) * 100\% \quad (10)$$

$$\text{Rate}: R_i(mmol/(g_{Ni}\cdot s)) = (F_{i,inlet} * X_i)/(m * w_{Ni}) \quad (11)$$

$$\text{Molar ratio of} H_2/CO: n_{H_2}/n_{co} = F_{H_2,outlet}/F_{CO,outlet} \quad (12)$$

$$\text{Carbon balance} C_{balance} = (F_{CH4,outlet} + F_{CO2,outlet} + F_{CO,outlet})/(F_{CH4,inlet} + F_{CO2,inlet}) \quad (13)$$

Where $F_{i,inlet}$, $F_{i,outlet}$ are flowrates of i species at the inlet and outlet respectively. m is the mass of catalyst and w_{Ni} is weight percentage of Ni in the catalyst.

When studying the influences of reaction conditions including catalyst mass, N_2 flow rate, Ni amount and CeO_2 amount for the microwave catalyzed MDR, the following experimental procedures were followed:

For the influence of catalyst mass, loadings of the 1Ni/CeO_2-SiC catalyst were changed to 20 mg, 30 mg and 40 mg while the microwave input, the ratio and flow rate of $CH_4/CO_2/N_2$, the reduction temperature and reduction time were the same as above. The conversions of CH_4 and CO_2 and the ratio of H_2/CO were measured from 873 K to 1023 K.

For the influence of N_2 flow, the flow rates of N_2 were varied to 10 mL/min, 20 mL/min, 30 mL/min and 40 mL/min when introducing $CH_4/CO_2/N_2$ mixture. The microwave input, the mass of the 1Ni/CeO_2-SiC catalyst, the ratio of $CH_4/CO_2/N_2$, the reduction temperature and reduction time were the same as above. The conversions of CH_4 and CO_2 and the ratio of H_2/CO were measured at 1023 K.

For the influences of Ni and CeO_2 amounts, MDR reaction over the Ni/CeO_2-SiC catalysts with Ni loadings of 1 %, 10 %, 15 % and 20 %, and 1Ni/xCeO_2-SiC (x presents the weight percentage of CeO_2) catalysts with CeO_2 loadings of 0 %, 5 %, 10 %, 20 % and 30 % were tested. The microwave input, the mass of the catalysts, the ratio and flow rate of $CH_4/CO_2/N_2$, the reduction temperature and reduction time were the same as above. The conversions of CH_4 and CO_2 and the ratio of H_2/CO were measured at 1023 K.

3. Results and discussion

3.1. Physical and chemical properties

ICP results suggest the same Ni loadings as the targeted values on the 1Ni/CeO_2-SiC, 3Ni/CeO_2-SiC and 5Ni/CeO_2-SiC catalysts (Table 1). N_2 adsorption-desorption of the reduced Ni/CeO_2-SiC catalysts (Fig. 1) display hysteresis loops, which are type IV of adsorption-desorption behaviors [26,27]. The loops confirm the mesoporous in the catalysts, as be evidenced by the inserted BJH pore size distribution plots. From the plots, average pore sizes are 12.7 nm, 13.2 nm and 12.8 nm in the reduced 1Ni/CeO_2-SiC, 3Ni/CeO_2-SiC and 5Ni/CeO_2-SiC catalysts, respectively, and their average pore volumes are corresponding to 0.010 cm^3/g, 0.011 cm^3/g, and 0.009 cm^3/g. The pores contribute to BET surface areas of 29.3 m^2/g, 26.6 m^2/g and 28.8 m^2/g for the reduced 1Ni/CeO_2-SiC, 3Ni/CeO_2-SiC and 5Ni/CeO_2-SiC catalysts, respectively.

XRD of the fresh Ni/CeO_2-SiC (Fig. 2) exhibits signals of 35.6°, 41.3°, 60.0°, 71.7° and 75.4° that attribute to (111), (200), (220), (311) and (222) crystal planes of SiC [18]. CeO_2 diffraction peaks are appeared at 28.5°, 33.0°, 47.6° and 56.4°, which are assigned to (111), (200), (220) and (311) crystal planes of CeO_2 [28]. The diffraction signals of NiO are not observed, which shall associate with the high dispersion of NiO or the Ni^{2+} species are embedded in lattice of ceria [29]. In the XRD patterns of reduced catalysts (Fig. 2), new composites of $Ce_{4.67}Si_3O_{13}$ are detected besides SiC. The new composite is originated from solid-solid reaction between partial SiC and CeO_{2-x} when the catalysts were reduced by H_2 at 1023 K [30]. This suggests that the SiC is not absolutely inert, it has some activity to interact with the reduced CeO_{2-x} to cerium silicate during H_2 treatment. In this sense, Ni-support interaction shall be more enhanced. Diffraction peaks of Ni are detected at 44.2 °C in the reduced Ni/CeO_2-SiC catalysts, indicating the reductions of NiO to metallic Ni.

H_2-TPR profile (Fig. 3) of SiC support doesn't show any reduction signals, which demonstrates the non-redox of SiC. When the Ni species are supported on the SiC, the reduction of individual NiO nanoparticles that have weak metal-support interaction are centered at 545 K, and the reduction of NiO that has strong metal-support interaction are peaked at 827 K [31]. As regards to the Ni/CeO_2-SiC catalysts, the first reduction begins from 550 K to 750 K, which is associated with the reduction of CeO_2 and reduction of partial individual NiO nanoparticles [32]. The

Table 1
Texture properties of the Ni/CeO_2-SiC catalysts.

Catalysts	Ni content (wt%)	Ni size (nm)[c]			BET (m^2/g)	Average pore size (nm)	Average pore volume (cm^3/g)
		Reduced	Used[a]	Used[b]			
1Ni/CeO_2-SiC	1.0	5.0	5.3	7.4	29.3	12.7	0.010
3Ni/CeO_2-SiC	3.0	8.1	7.9	8.5	26.6	13.2	0.011
5Ni/CeO_2-SiC	5.0	9.0	11.3	14.3	28.8	12.8	0.009
3Ni/SiC	3.0	8.0	10.5	13.3	–	–	–

Note: a: Ni size of the used catalysts after microwave catalysis; b: Ni size of the used catalysts after traditional thermal catalysis; c: the Ni sizes are obtained from XRD patterns of the catalysts.

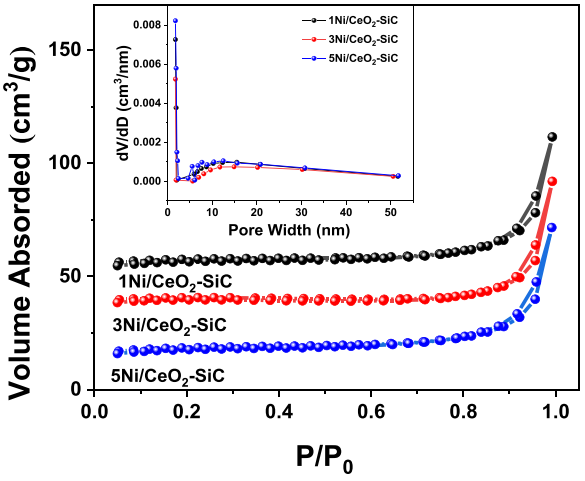

Fig. 1. N_2 adsorption-desorption curves and BJH pore size distributions of the reduced Ni/CeO_2-SiC catalysts.

second reduction starts at 750–1000 K, which may be owned to the reduction of resting NiO nanoparticles that has strong metal-support interaction with SiC, as well as the oxygen removal from cerium silicate $Ce_{4.67}Si_3O_{13}$ when partial active reduced CeO_{2-x} is interacting with partial active SiC [31]. The blue-shifted reduction temperatures in the Ni/CeO_2-SiC catalysts suggest that the addition of CeO_2 strengthened the metal-support interaction between Ni and SiC, most properly in the form of $Ce_{4.67}Si_3O_{13}$. The stronger metal-support interaction on the Ni/CeO_2-SiC is demonstrated by H_2-TPD (Fig. S2, Table S1), in which the desorption temperatures were slightly higher and the amounts of chemical-adsorbed hydrogen was lower than those in the reference Ni/SiC. It is expected that this stronger interaction will more chemically confine Ni nanoparticles on SiC, inhibiting Ni aggregation and sintering.

HRTEM of the reduced Ni/CeO_2-SiC (Fig. 4) show the distribution of Ni nanoparticles on SiC surface. The lattice spacings of Ni nanoparticles and SiC support are 0.20 nm and 0.25 nm, corresponding to Ni(111) and SiC(111), respectively. The SiC has not a particular shape, while the Ni nanoparticles are spheres. The boundary between Ni nanoparticles and SiC support provides sites for molecules activation and intermediates transformation. Average sizes of Ni nanoparticles are 5.0 nm, 8.1 nm and 9.0 nm on the 1Ni/CeO_2-SiC, 3Ni/CeO_2-SiC and 5Ni/CeO_2-SiC, respectively (Fig. S3).

The representative reduced 3Ni/CeO_2-SiC catalyst is applied to analysis surface compositions by XPS. The fine XPS of Ni 2p3/2 (Fig. 5, A) depicts three signals at 852.7 eV and 855.6 eV, which are ascribed to species of Ni^0 and Ni^{2+}, respectively, and the satellite peak of Ni^0 2p3/2 locates at 861.6 eV [33]. The detection of Ni^{2+} indicates the residual Ni^{2+} on catalyst surface, which may from the oxidation of metallic Ni before introducing to XPS chamber. The XPS of Ce 3d (Fig. 5, B) are fitted to ten peaks, where v and u represent the spin-orbit couplings $3d_{3/2}$ and $3d_{5/2}$, respectively. Among the peaks, v′ and u’ are from Ce^{3+}, while other peaks are from Ce^{4+} [7,34]. Due to the Ce element is composed in cerium silicate but not CeO_2, the signals of u’’’ in the used samples are different with that in CeO_2. This confirms that the bonding energy of Ce^{4+} $3d_{5/2}$ is affected by the silicate. To further study the formation of the cerium silicate phase, the O ls XPS spectra of the reduced samples are analysed (Fig. 5, C). The O ls XPS spectra of the reduced samples are composed of three peaks. The first peak locating at 529.4 eV is related to surface lattice oxygen in Ce-O, the second signal at 530.6 eV is associated with oxygen atom in a cerium silicate phase [30]. The silicate is most properly from the interaction between ceria and active SiC, implying that the catalyst undergoes interfacial reaction to form cerium silicate, in good consistent with previous XRD results. The third O 1 s peak at 532.8 eV is assigned to oxygen bonding to Si^{4+} [4,

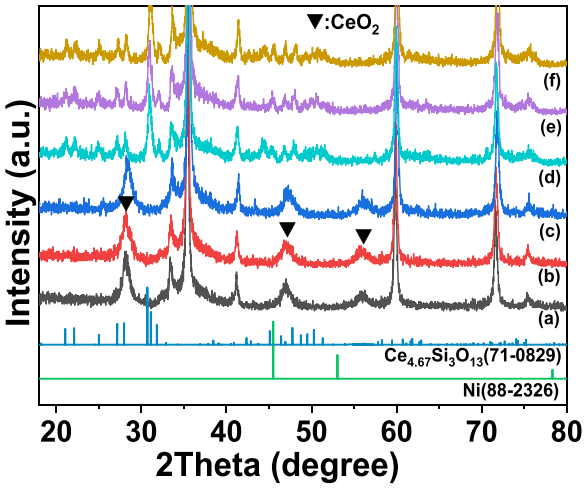

Fig. 2. XRD patterns of fresh (a)1Ni/CeO_2-SiC, (b)3Ni/CeO_2-SiC, (c)5Ni/CeO_2-SiC catalysts, and reduced (d) 1Ni/CeO_2-SiC catalysts, (e) 3Ni/CeO_2-SiC and (f) 5Ni/CeO_2-SiC catalysts.

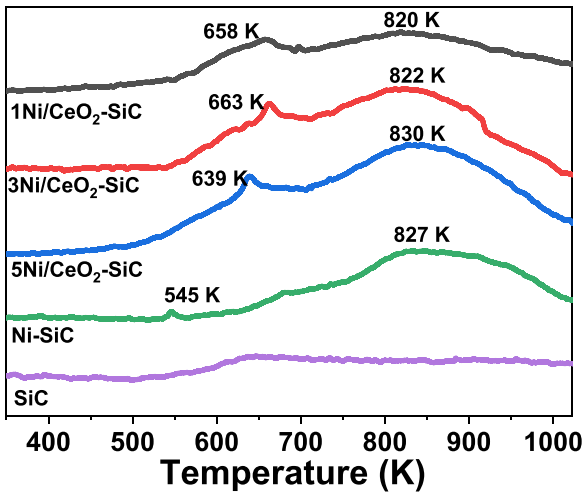

Fig. 3. H_2-TPR of the fresh Ni/CeO_2-SiC catalysts, reference Ni-SiC sample and pure SiC.

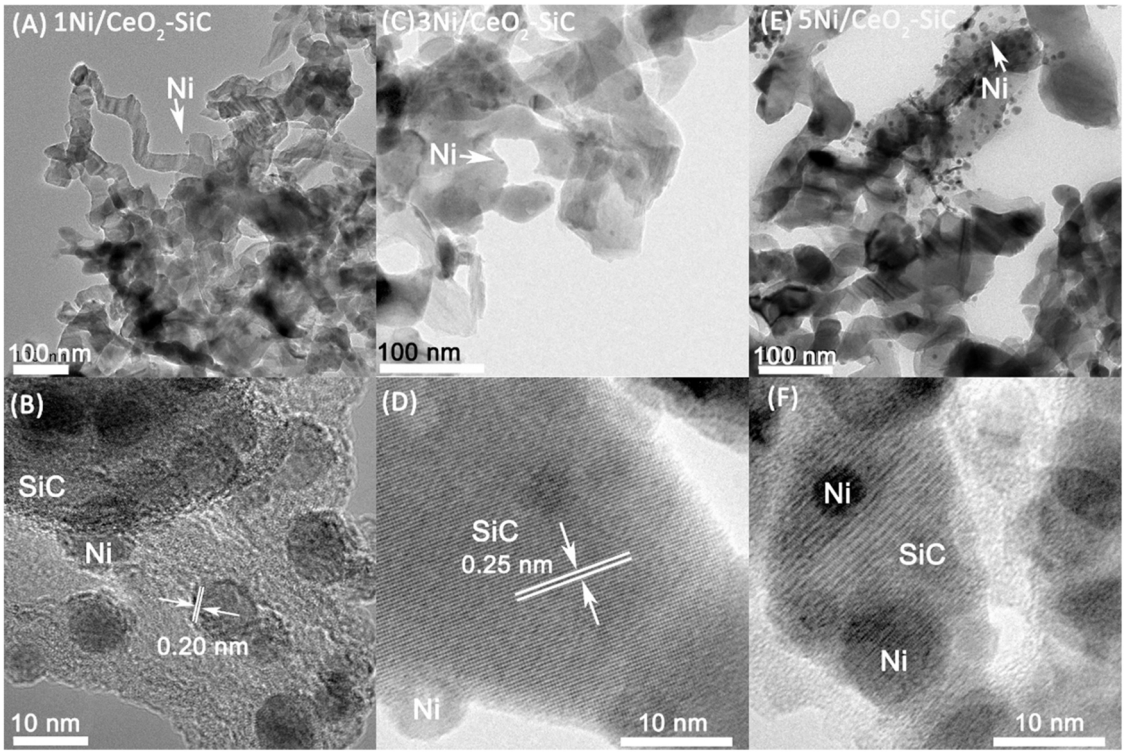

Fig. 4. HRTEM of the reduced (A, B) 1Ni/CeO_2-SiC, (C, D)3Ni/CeO_2-SiC, (E, F)5Ni/CeO_2-SiC catalysts.

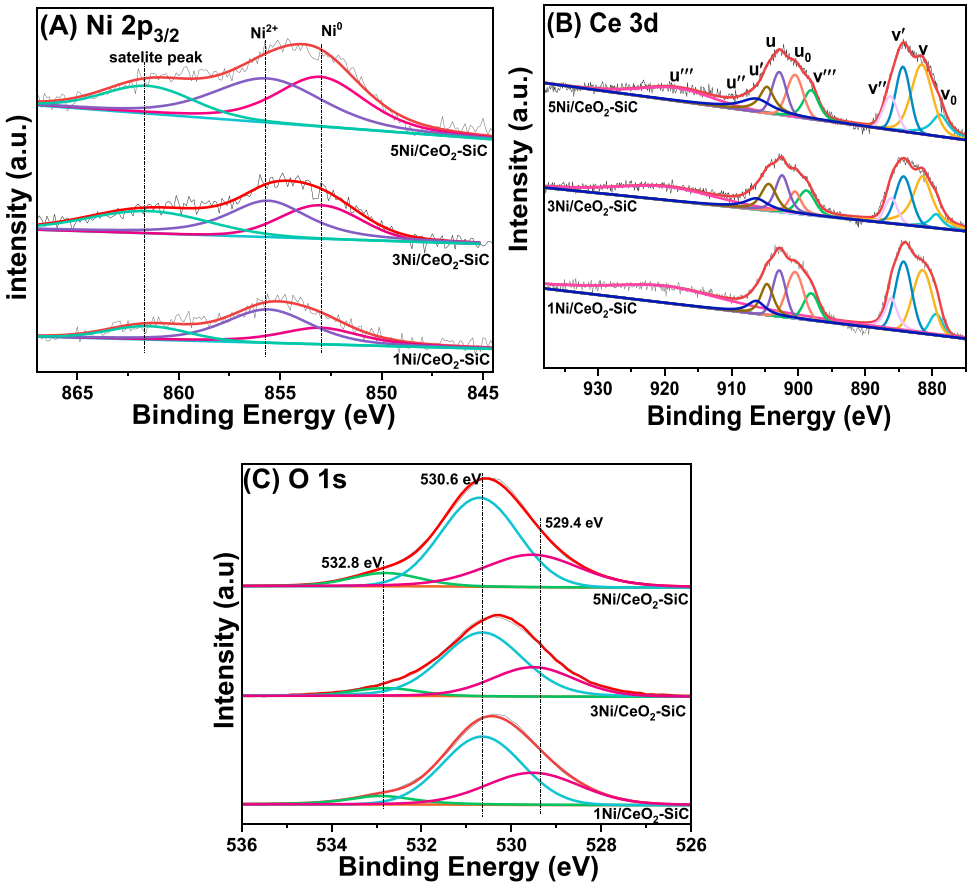

Fig. 5. XPS analysis of the reduced 3Ni/CeO_2-SiC. (A) Ni 2p3/2, (B) Ce 3d, (C) O 1s.

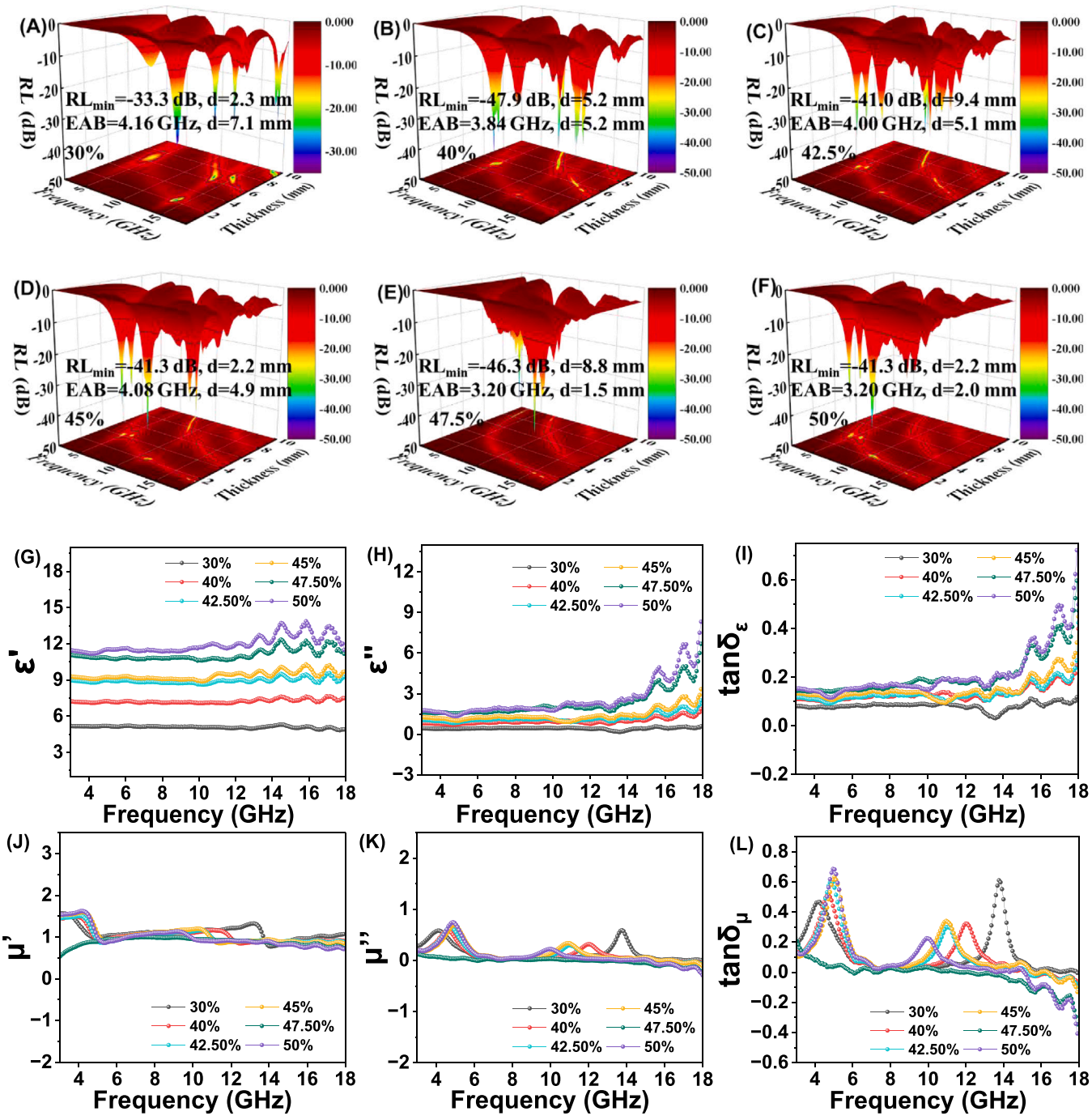

Fig. 6. (A–F) 3-D graph of microwave absorption performance of the reduced 3Ni/CeO_2-SiC. (G) ε′, (H) ε″, (I) tanδε, (J) μ', (K) μ'' and (L) tanδμ as a function of frequency.

35]. The above results are consistent with previously XRD that the interfacial interaction between SiC and CeO_2 was happened during high temperature reduction treatment.

3.2. Electromagnetic wave absorption performance

Electromagnetic wave absorption performance of the 3Ni/CeO_2-SiC is evaluated by Reflection Loss (RL, Fig. 6, A–F) [36]. The result reveals that RL_{min} is between − 33.3 dB and − 47.9 dB when varying the thickness between 2.2 mm and 8.8 mm. The highest RL_{min} is − 47.9 dB at thickness 5.2 nm. Due to 99 % microwave can be adsorbed at RL < −10 dB, the result confirms that the Ni/CeO_2-SiC can indeed adsorb microwave energy, and the maximum adsorption beyond 99.99 % at RL < −30 dB. This is also verified by the circled regions adsorbing microwave higher than 99 % in 3D RL projection images (Fig. S4, A1–F1). The RL-frequency curves (Fig. S4, A2–F2) suggest that absorption bandwidth (EAB) of the sample is above 3.20 GHz at thicknesses 1–10 mm. These confirm that the 3Ni/CeO_2-SiC satisfies the requirement of high RL at lower thickness and large EAB for perfect microwave adsorption [37]. When correlating to components in the projection images, the red regions have the lowest RL, which shall from the microwave adsorption by SiC; the green-blue regions have the highest RL, which ought to associate with the microwave adsorptions by Ni and SiC. The yellow regions are between the regions of red and green-blue, which are attributed to

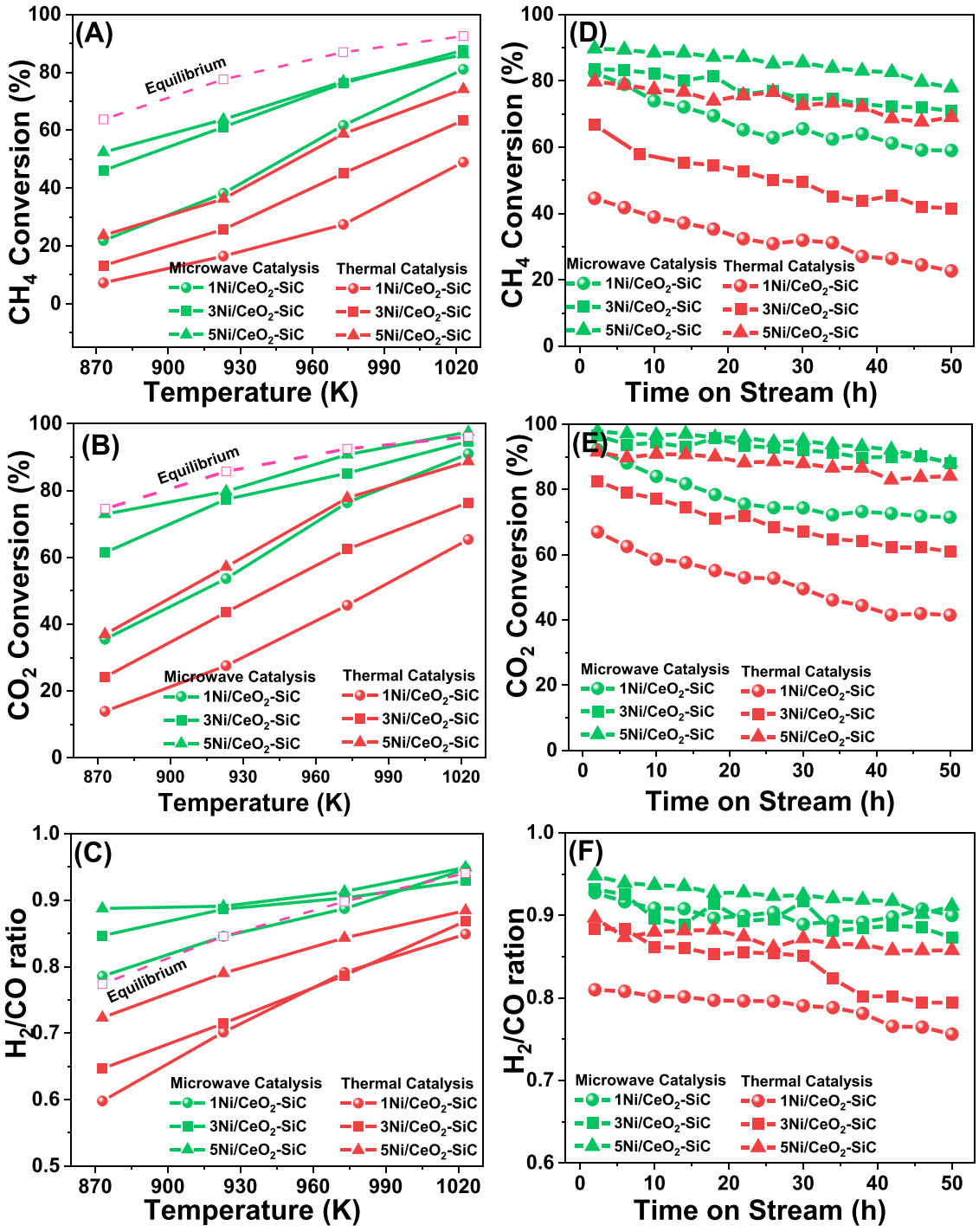

Fig. 7. MDR activity (A-C) and stability (D-F) over the Ni/CeO_2-SiC catalysts by microwave catalysis and thermal catalysis. (A. D): CH_4 conversion, (B, E): CO_2 conversion and (C, F): H_2/CO ratio. (Reaction condition: catalyst 50 mg, molar ratio $CH_4/CO_2/N_2$ = 3/3/4, GHSV=60 L/(gh), targeted temperature 873–1023 K).

microwave adsorption at Ni-support interface. Due to the transformation of adsorbed microwave energy to heat energy, the temperatures of Ni and Ni-support interface shall be higher under microwave irradiation than those provided by electric furnace. The temperature enhancement shall complement heat loss from endothermic MDR on catalyst, benefiting to increase performance and reduce carbon deposition.

The heating property of the catalyst under microwave irradiation were further verified by magnetic loss (μ") and dielectric loss factor ($\tan\delta_\varepsilon = \varepsilon"/\varepsilon'$) as a function of frequency. Generally, the real parts ε′ and μ' are associated storage ability, and the imaginary parts of ε″ and μ'' are related to attenuation ability of electric energy and magnetic energy, respectively [38]. The dielectric loss capability of the 3Ni/CeO_2-SiC catalyst with weight percentages from 30 % to 50 % (Fig. 6, G–I) reveal that ε′ and ε" are both increased with the weight percentage, indicating that the more 3Ni/CeO_2-SiC shall have the higher storage and attenuation capacity of dielectric energy. The increased values of ε″ and $\tan\delta_\varepsilon$ at high frequency of 15–18 GHz suggest the presence of multiple polarization process, while their multiple peaks are owed to the difference of dipole orientation [39]. The higher $\tan\delta_\varepsilon$ at the higher weight percentage implies the higher attenuation of microwave energy to heat. The magnetic loss capability of the 3Ni/CeO_2-SiC (Fig. 6, J–L) shows the

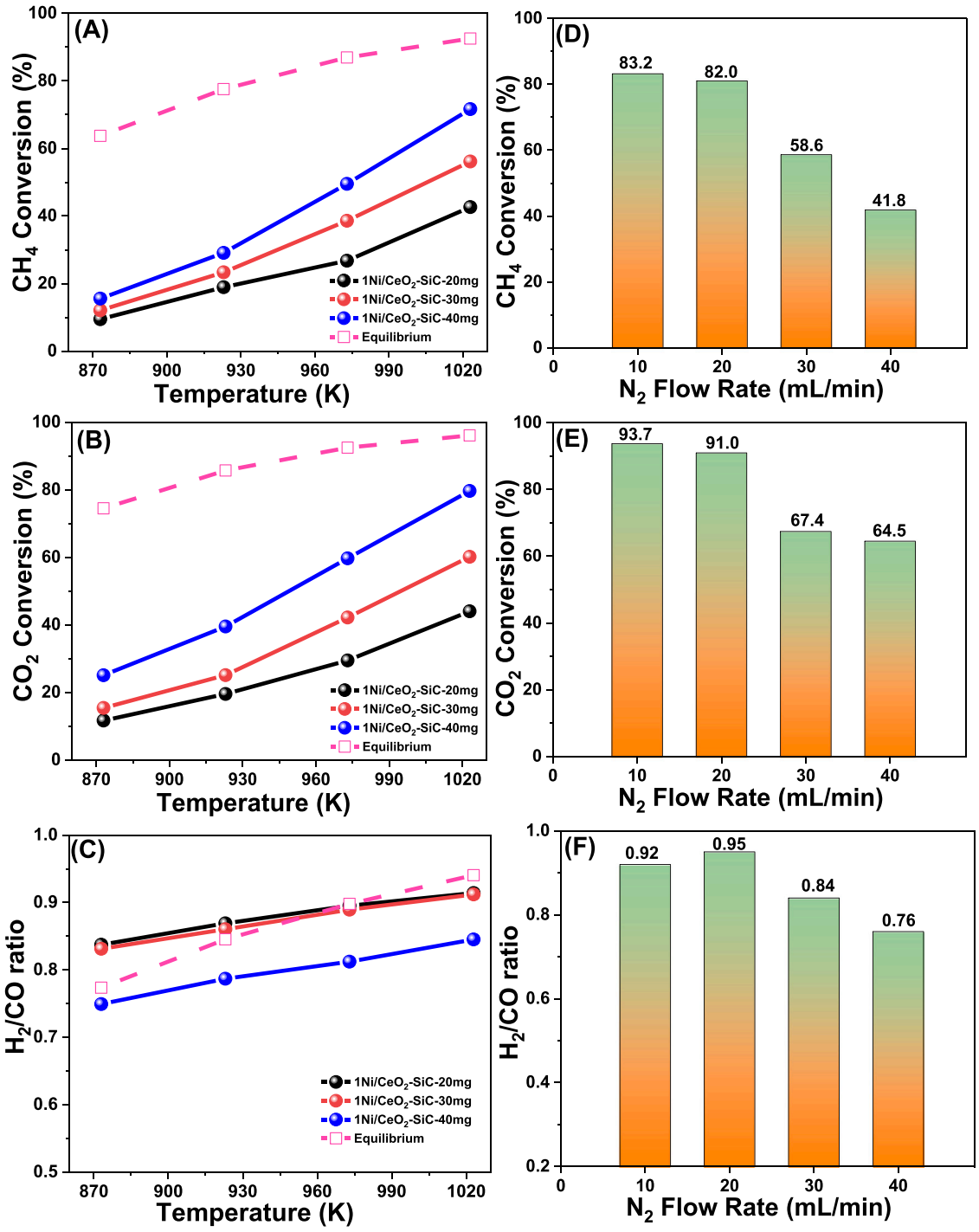

Fig. 8. Influences of (A–C) catalyst mass and (D-F) N_2 flow rate on microwave catalytic performance of MDR over the 1Ni/CeO_2-SiC catalysts. (A, D) CH_4 conversion, (B, E) CO_2 conversion and (C, F) H_2/CO ratio. (Reaction condition: A-C: catalyst 20–40 mg, molar ratio $CH_4/CO_2/N_2$ =3/3/4, GHSV=60 L/(gh), targeted temperature 873–1023 K; D-F: catalyst 50 mg, molar ratio $CH_4/CO_2/N_2$ = 3/3/4, N_2 = 10–40 mL/min, targeted temperature 1023 K).

fluctuations of μ″ and tanδμ with frequencies. The low frequency fluctuations are due to natural resonances and the high frequency fluctuations are from exchange resonances. The negative values of μ″ and tanδμ in high frequency are because of the induced magnetic field generation and the radiation of magnetic energy. The more negative of μ″ again confirms the higher attenuation ability of magnetic energy to heat [40].

3.3. Microwave catalytic performance of MDR

MDR activity (Fig. 7, A–C) results reveal that CH_4 conversions were 7.2 % 13.2 % and 23.6 % over the 1Ni/CeO_2-SiC, 3Ni/CeO_2-SiC and 5Ni/CeO_2-SiC, respectively, at 873 K in traditional thermal catalysis. The values were accordingly increased to 48.9 %, 63.4 % and 74.2 % at 1023 K. Similarly, CO_2 conversions were 13.9 %, 24.1 % and 36.9 % at 873 K, and were enhanced to 65.3 %, 76.4 % and 88.7 % at 1023 K over the corresponding Ni/CeO_2-SiC. In contrast to microwave catalysis, CH_4 conversions were 21.8 %, 46.1 % and 52.4 % at 873 K, and were promoted 81.0 %, 87.6 % and 86.2 % at 1023 K over the 1Ni/CeO_2-SiC, 3Ni/CeO_2-SiC and 5Ni/CeO_2-SiC, respectively. CO_2 conversions were 35.5 %, 61.4 % and 72.9 % at 873 K, and were increased to 91.0 %, 94.7

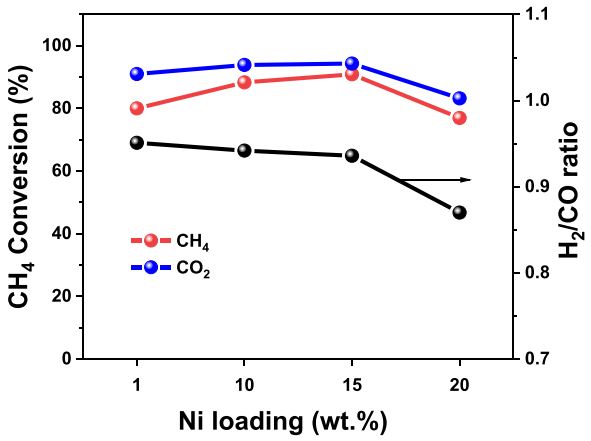

Fig. 9. Influence of Ni loading on the Ni/CeO_2-SiC catalysts for microwave catalytic performance of MDR. (Reaction condition: catalyst 50 mg, molar ratio $CH_4/CO_2/N_2$ = 3/3/4, GHSV=60 L/(gh), targeted temperature 1023 K).

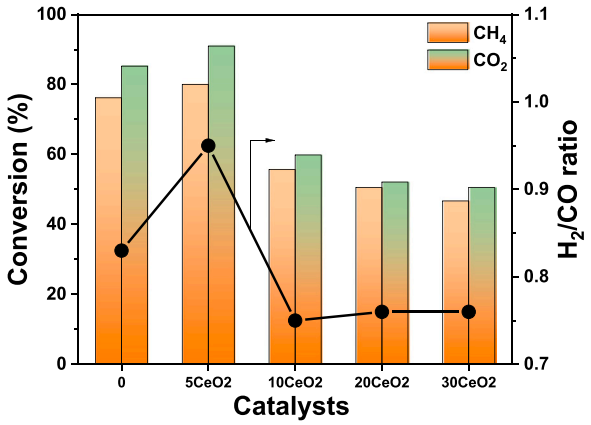

Fig. 10. Influence of CeO_2 loadings on the 1Ni/xCeO_2-SiC (x presents the weight percentage of CeO_2) catalysts for microwave catalytic performance of MDR. (Reaction condition: catalyst 50 mg, molar ratio $CH_4/CO_2/N_2$ =3/3/4, GHSV=60 L/(gh), targeted temperature 1023 K).

% and 97.5 % at 1023 K. In all the cases, CO_2 conversions were higher than CH_4, which was related to reverse water gas shift (RWGS, $CO_2+H_2 \rightarrow CO+H_2O$) [41], giving H_2/CO ratio below equilibrium in thermal catalysis. However, the ratio was above in microwave catalysis, suggesting the happening of methane steam reforming ($CH_4+H_2O \rightarrow CO+3\ H_2$) besides RWGS under microwave irradiation. Carbon balances were between 95 % and 105 % in the tests (Fig. S5), suggesting the not serious carbon deposition.

The above evidences the higher MDR activity by microwave catalysis than by thermal catalysis over the Ni/CeO_2-SiC catalysts, which shall associate with the more effective energy efficiency by microwave irradiation (Table S2, in which the energy efficiencies are 30.7–57.3 %, 41.6–60.8 % and 11.9–55.0 % for the catalysts of 1Ni/CeO_2-SiC, 3Ni/CeO_2-SiC and 5Ni/CeO_2-SiC, respectively, by thermal catalysis from 873 K to 1023 K. The efficiencies are slightly lower than those of 50.7–63.4 %, 62.3–64.6 % and 48.1–63.2 % for the corresponding catalysts by microwave catalysis.) and the transfer of adsorbed microwave energy to heat energy by Ni and SiC, leading to higher temperature of catalyst in microwave catalysis than in thermal catalysis (Fig. S6, in which catalyst surface temperature is increased about 100–120 K in microwave catalysis compared to in thermal catalysis.). Meanwhile, the lower apparent E_a of CH_4 and CO_2 by microwave catalysis (Fig. S7, Table S3) reasonably explain the higher MDR activity than by thermal catalysis. The possible mechanism may be due to that the adsorption of electromagnetic wave changes the internal energy levels of CH_4 and CO_2 by interaction between microwave with SiC and Ni, decreasing their activation barriers and accelerating their rates. This is different from the temperature effect in promoting rates in conventional electronic furnace heating, indicating that microwave effect rather than heating effect decreases the activation energies [42–44]. It should be noticed that E_a of CH_4 was lower than CO_2 for both microwave and thermal catalysis. According to literatures, the possible explanations might be the changed rate-determining step from C-H activation in CH_4 to diffusion of reactants or production of CO. The former might because of the very high GHSV when conducting the kinetic measurements [45], and the latter might associated with the lower E_a of CH_4 and CO_2 than that of CO [46].

The stability tests (Fig. 7, D–F) show that conversions of CH_4 and CO_2, ratio of H_2/CO, were marginally changed under microwave irradiation, while their faster decays were observed in traditional thermal catalysis. These confirm the more stable of MDR by Ni/CeO_2-SiC in microwave catalysis than in thermal catalysis.

The influence of catalyst mass on the microwave catalytic performance of MDR over the 1Ni/CeO_2-SiC catalysts (Fig. 8, A–C) suggests that the conversions of CH_4 and CO_2 are increased with the increment of catalyst mass. This shall be originated from the more presences of Ni and SiC, which positively increasing active sites and enhancing the microwave adsorbing, respectively. These consequently promoted the activations and transformations of CH_4 and CO_2. The molar ratios of H_2/CO

Table 2
Comparisons of CH_4 and CO_2 rates between the Ni/CeO_2-SiC catalysts and the published results.

Catalysts	Reaction Conditions				CH_4 rate (mmol/ (g_{Ni}·s))	CO_2 rate (mmol/ (g_{Ni}·s))	Ref.
	Catalysis	Temp. (K)	GHSV (L/gh)	$CH_4/CO_2/N_2$			
1Ni/CeO_2-SiC	Microwave	1023	60	3/3/4	16.53	18.57	This work
3Ni/CeO_2-SiC		1023	60	3/3/4	5.96	6.44	
5Ni/CeO_2-SiC		1023	60	3/3/4	3.51	3.98	
Ni/$CeAlO_3$- Al_2O_3/SCF		1123	24	1/1/1	1.50	1.76	[19]
FY5 + Ni/Al_2O_3		1123	1.5	1/1/0	0.15	0.17	[47]
LSC-Mn		973	24	1/1/0	1.08	1.08	[48]
Ni-STU		973	72	2/2/6	1.37	1.42	[49]
2Ni-La/AC		973	9.6	15/15/70	0.81	0.81	[50]
1Ni/CeO_2-SiC	Thermal	1023	60	3/3/4	9.99	13.33	This work
3Ni/CeO_2-SiC		1023	60	3/3/4	4.31	5.20	
5Ni/CeO_2-SiC		1023	60	3/3/4	3.03	3.62	
NHS-SiO_2-S		1023	24	1/1	0.51	0.46	[51]
NiMo/MgO		1073	60	1/1/8	1.81	1.81	[52]
Ni/20CeO_2		973	30	1/1/2	4.87	5.25	[53]
Ni/h-BN		973	60	2/2/1	5.16	5.76	[54]
NiSiCart		973	22.5	2/2/1	1.91	2.19	[55]
Ni/MgO-mSiO_2		973	275	1/1/8	2.08	2.15	[56]

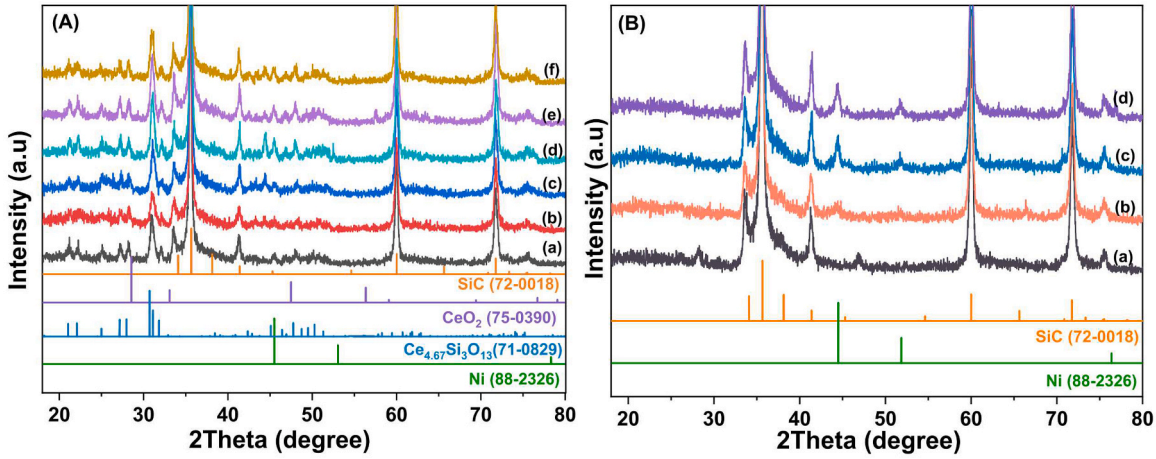

Fig. 11. (A) XRD patterns of used Ni/CeO_2-SiC after MDR stability by thermal and microwave catalysis. Thermal catalysis samples: (a) 1Ni/CeO_2-SiC, (b) 3Ni/CeO_2-SiC and (c) 5Ni/CeO_2-SiC; microwave catalysis samples: (d) 1Ni/CeO_2-SiC, (e) 3Ni/CeO_2-SiC and (f) 5Ni/CeO_2-SiC. (B) XRD of 3Ni/SiC reference catalysts. (a) fresh sample, (b) reduced sample, (c) used sample after thermal catalysis, (d) used sample after microwave catalysis.

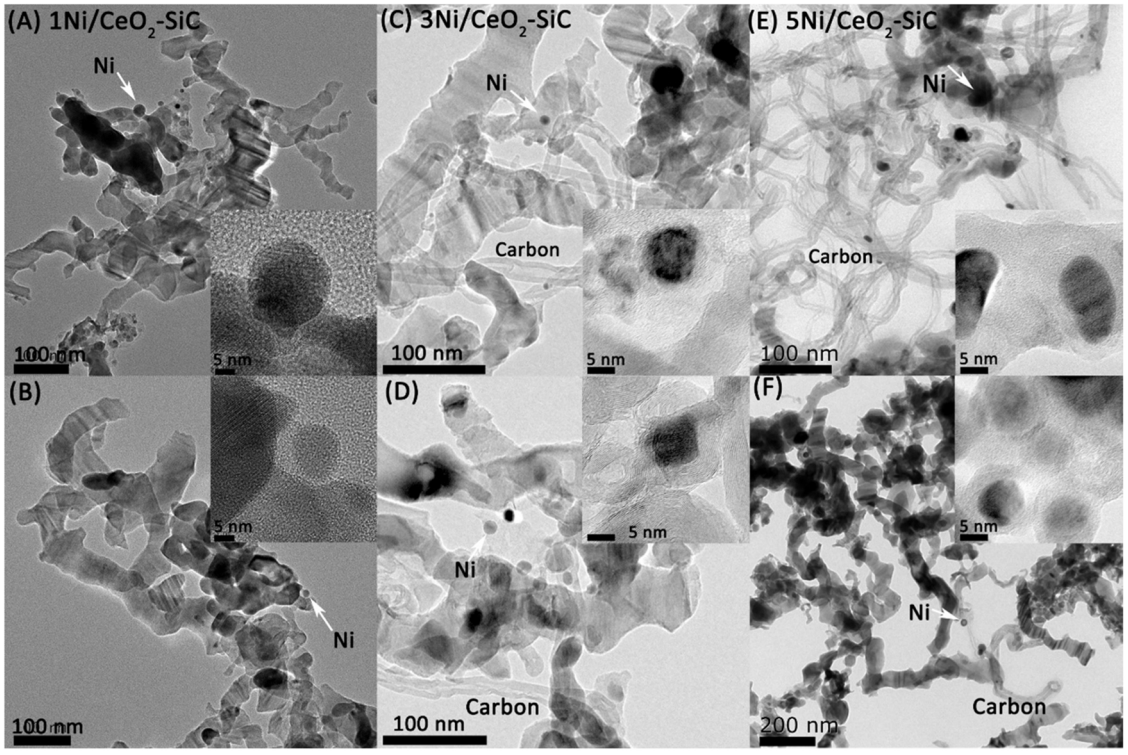

Fig. 12. HRTEM images of used Ni/CeO_2-SiC catalysts. (A, C, E): thermal catalysis, (B, D, F): microwave catalysis.

are identical when using 20 mg and 30 mg catalyst, but is considerably decreased when using 40 mg catalyst. This may be explained from that the more mass usage favors the happening of reverse water gas shift reaction. The flow rate of N_2 is also observed influencing the microwave catalytic performance of MDR (Fig. 8, D–F). The conversions of CH_4 and CO_2, as well as the ratios of H_2/CO, are progressively decreased with the increment of N_2 flow rate. This shall be owned to the decreased the partial pressures of CH_4 and CO_2, as well as the shortened the contact time, when increasing N_2 flow rate.

The influence of Ni loading on the microwave catalytic performance of MDR (Fig. 9) show that the conversions of methane CH_4 and CO_2 are firstly increased from the 1Ni/5CeO_2-SiC to the 15Ni-5CeO_2/SiC catalysts, and then decreased from the 15Ni/5CeO_2-SiC to the 20Ni/5CeO_2-SiC catalysts. The former increment may be due to the higher loading of Ni that displays positive promotion in the conversions, while the latter decrement shall be owned to the further higher loading of Ni forming bigger Ni sizes (Fig. S8) and thus exhibiting negative influence. Therefore, if we considered the conversions of CH_4 and CO_2, the optimized Ni loading shall 15 % in the current study. However, if we considered the rates of CH_4 and CO_2 per mass of Ni, the highest rates are given by the catalyst with Ni loading of 1 %, which can be verified in the following Table 2. As regards to the ratio of H_2/CO, methane conversion is increased but H_2/CO is decreased when Ni loading is less than 15 wt%, this shall relate to the happening of reverse water gas shift reaction ($CO_2+H_2 \rightarrow CO+H_2O$). Above Ni loading of 15 wt%, the continuous decrease of H_2/CO ratio shall associate with the decrease of methane conversion and the occurrence of reverse water gas shift reaction.

The influence of CeO_2 loading on the microwave catalytic

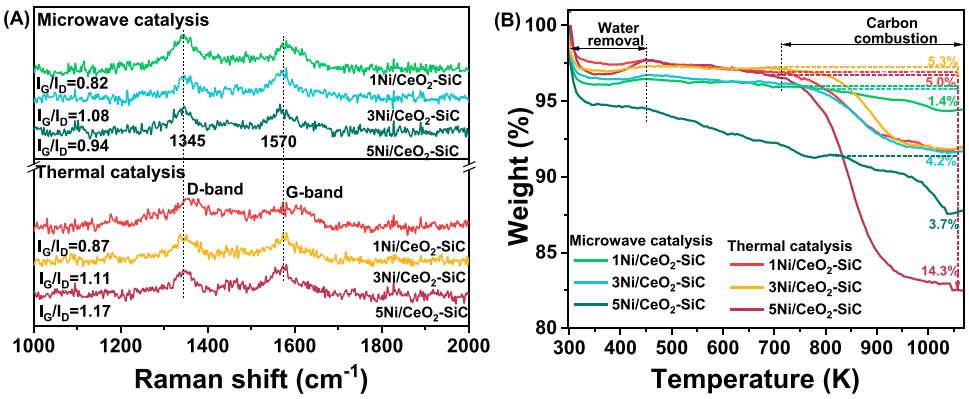

Fig. 13. (A) Raman and (B) TG of the used Ni/CeO_2-SiC catalysts.

performance of MDR is also analysed. The results (Fig. 10) show that the conversions of CH_4 and CO_2, as well as the H_2/CO ratio, are increased from the 1Ni/SiC catalyst without CeO_2 to the 1Ni/5CeO_2-SiC catalyst with 5 wt% CeO_2, then are decreased from the 1Ni/5CeO_2-SiC to 1Ni/30CeO_2-SiC. The possible explanation may be associated with the strong metal-support interaction in the catalyst when adding more CeO_2. As be verified from the H_2-TPR profiles (Fig. S9), the full reductions of Ni species on the 1Ni/5CeO_2-SiC, 1Ni/10CeO_2-SiC and 1Ni/15CeO_2-SiC need temperatures of 1046 K, 1084 K and 1106 K, respectively. Due to the reduction treatment temperature is only 1023 K before conducting MDR, the higher loading of CeO_2 result in the fewer reduction of Ni species because of the much-enhanced metal-support interaction. In this case, the fewer Ni atoms shall be exposed for the lower MDR performance at the higher CeO_2 loading. Besides, the lower surface temperatures when adding more CeO_2 on the Ni/CeO_2-SiC catalysts give another explanation for the decreased performance. As be evidenced from the surface temperature measurements (Fig. S10), the temperature of the 1Ni/30CeO_2-SiC catalyst is about 40 K lower than that of the 1Ni/5CeO_2-SiC catalyst. The origination may associate with the more formation of $Ce_{4.67}Si_3O_{13}$ when adding higher CeO_2 reacting with more SiC. The $Ce_{4.67}Si_3O_{13}$ shall have low ability to adsorb microwave and the less remaining SiC attenuates the adsorption of microwave.

CH_4 and CO_2 rates are compared with published results (Table 2). The 1Ni/CeO_2-SiC has the highest CH_4 and CO_2 rates of 16.5 mmol/(g_{Ni}·s) and 18.6 mmol/(g_{Ni}·s), respectively, under microwave irradiation at 1023 K, followed by the 3Ni/CeO_2-SiC and 5Ni/CeO_2-SiC. The higher rates were obtained at the catalyst with the lower Ni loading, which is because the similar CH_4/CO_2 conversions but the multiple differences of Ni contents. Compared with the reported rates in microwave catalysis, the rates were order-of-magnitude increased exhibiting the excellent activity. Although the rates in thermal catalysis were not as high as those in microwave catalysis, they were also higher than most published results.

3.4. Characterizations of used catalysts

XRD of the used samples (Fig. 11, A) show main diffraction peaks assigned to Ni, SiC and $Ce_{4.67}Si_3O_{13}$. The Ni sizes in the used samples were slightly increased when compared with those in the reduced ones (Table 1), suggesting the slight agglomeration of Ni. The relative higher aggregation under microwave irradiation ought to associate with the higher surface temperature of the Ni/CeO_2-SiC catalysts in microwave catalysis than in thermal catalysis. However, contrast to the more significant Ni aggregation in used Ni/SiC catalysts without CeO_2 (Fig. 11, B), the aggregation in the Ni/CeO_2-SiC was much alleviated because of the enhanced metal-support interaction induced by CeO_2.

Carbon was not observed in TEM the images of the used 1Ni/CeO_2-SiC after thermal catalysis (Fig. 12, A, C, E), but was seen on the used 3Ni/CeO_2-SiC and 5Ni/CeO_2-SiC. Some Ni were on the tip of carbon nanotubes, and some were covered by carbon graphite. The formation of the carbon deposits should from deep cracking of CH_x diffused through Ni crystals, some atoms nucleated and grew to carbon nanotubes, and some atoms clustered and aggregated to graphite [57]. The carbon covering Ni surfaces is one cause to decay MDR performance in thermal catalysis. Statistically, average Ni sizes were 7.4 nm, 8.5 nm and 14.3 nm on the used 1Ni/CeO_2-SiC, 3Ni/CeO_2-SiC and 5Ni/CeO_2-SiC (Fig. S10, A–C), respectively, the slight Ni sintering contributed to another cause to decay thermal performance. For the used samples after microwave catalysis (Fig. 12, B, D, F), carbon nanotube and graphite were also formed on the 3Ni/CeO_2-SiC and 5Ni/CeO_2-SiC but not 1Ni/CeO_2-SiC. In a literature, carbon deposits can adsorb microwave increasing catalyst surface temperature, and the carbon atoms can be intermediates to produce CO in MDR [58]. The properties explained the more stable enhanced MDR performance by microwave catalysis. Average Ni sizes on the used 1Ni/CeO_2-SiC, 3Ni/CeO_2-SiC and 5Ni/CeO_2-SiC were 5.3 nm, 7.9 nm and 11.3 nm (Fig. S10, D–F), respectively, evidencing the much-alleviated Ni sintering in microwave MDR.

The nature and amounts of the carbon deposits are analysed by Raman and TG. In the Raman spectra (Fig. 13, A), the peak of 1345 cm^{-1} (D band) is associated with disordered carbon and the peak of 1570 cm^{-1} (G band) is related to graphitic carbon [1]. The ratios of I_G/I_D, an indication of graphitization degree of the carbon, are 0.82, 1.08, and 0.94 for the used 1Ni/CeO_2-SiC, 3Ni/CeO_2-SiC and 5Ni/CeO_2-SiC, respectively, after microwave catalysis stability. The ratios are slightly lower than corresponding 0.87, 1.11 and 1.17 for the used catalysts after thermal catalysis, verifying the lower graphitization degree of carbon under microwave irradiation [59]. In the TG spectra (Fig. 13, B), the weight loss at 300–400 K is from removal of adsorbed water, and the rapid weight loss at 700–1023 K is from carbon combustion [32]. Carbon deposits are 5.0 wt%, 5.3 wt% and 14.3 wt% on the used 1Ni/CeO_2-SiC, 3Ni/CeO_2-SiC and 5Ni/CeO_2-SiC, respectively, after thermal stability tests, in contrast to corresponding 1.4 wt%, 4.2 wt % and 3.7 wt% on the used samples after microwave stability tests. These evidence that carbon was less deposited on the catalysts in microwave catalysis, which is related to the higher catalyst surface temperature promoting the gasification of carbon precursors. As a consequence, MDR stability over the Ni/CeO_2-SiC catalysts was much strengthened in microwave catalysis.

4. Conclusion

As a summary, Ni/CeO_2-SiC catalysts are newly developed for MDR by microwave catalysis compared to thermal catalysis. The lower activation energies of CH_4 and CO_2, and the higher catalyst surface temperature are realized by microwave irradiation than those in conventional thermal catalysis. These contribute to the more stable higher MDR performance and the less carbon deposition on the Ni/

CeO_2-SiC catalysts in microwave catalysis than in traditional thermal catalysis. CH_4 and CO_2 rates were one order-of-magnitude increased, showing the great advantages of microwave catalysis. Carbon deposits were minimized to 1.4 wt% by microwave catalysis compared to 5.0 wt % by thermal catalysis. The work verifies that microwave catalysis is more advance for MDR than thermal catalysis over the Ni/CeO_2-SiC catalysts, which is suitable for other microwave-adsorbed catalysts catalyzing other reactions.

CRediT authorship contribution statement

Yu Shi: Investigation, Methodology, Data curation, Formal analysis, Writing – original draft. **Lei Wang:** Methodology, Data curation. **Mengmeng Wu:** Resources, Supervision. **Fagen Wang:** Conceptualization, Formal analysis, Funding acquisition, Resources, Supervision, Writing – review & editing.

Declaration of Competing Interest

The authors declare that they have no known competing financial interests or personal relationships that could have appeared to influence the work reported in this paper.

Data Availability

Data will be made available on request.

Acknowledgement

The work is supported by National Natural Science Foundation of China (22078134), State Key Laboratory of Clean and Efficient Coal Utilization of Taiyuan University of Technology (SKL2022006) and Postgraduate Research & Practice Innovation Program of Jiangsu Province (SJCX23_2075).

Appendix A. Supporting information

Supplementary data associated with this article can be found in the online version at doi:10.1016/j.apcatb.2023.122927.

References

[1] K. Han, S. Wang, N. Hu, W. Shi, F. Wang, Alloying Ni–Cu nanoparticles encapsulated in SiO_2 nanospheres for synergistic catalysts in CO_2 reforming with methane reaction, ACS Appl. Mater. Interfaces 14 (2022) 23487–23495.
[2] L. Wang, F. Wang, Design strategy, synthesis, and mechanism of Ni catalysts for methane dry reforming reaction: recent advances and future perspectives, Energy Fuels 36 (2022) 5594–5621.
[3] C.M. Damaskinos, J. Zavašnik, P. Djinović, A.M. Efstathiou, Dry reforming of methane over Ni/$Ce_{0.8}Ti_{0.2}O_{2-\delta}$: the effect of Ni particle size on the carbon pathways studied by transient and isotopic techniques, Appl. Catal. B: Environ. 296 (2021), 120321.
[4] D. Guo, Y. Lu, Y. Ruan, Y. Zhao, Y. Zhao, S. Wang, X. Ma, Effects of extrinsic defects originating from the interfacial reaction of CeO_{2-x}-nickel silicate on catalytic performance in methane dry reforming, Appl. Catal. B: Environ. 277 (2020), 119278.
[5] K. Lorber, J. Zavašnik, J. Sancho-Parramon, M. Bubaš, M. Mazaj, P. Djinović, On the mechanism of visible-light accelerated methane dry reforming reaction over Ni/CeO_{2-x} catalysts, Appl. Catal. B: Environ. 301 (2022), 120745.
[6] F. Wang, B. Han, L. Zhang, L. Xu, H. Yu, W. Shi, CO_2 reforming with methane over small-sized Ni@SiO_2 catalysts with unique features of sintering-free and low carbon, Appl. Catal. B: Environ. 235 (2018) 26–35.
[7] F. Wang, L. Xu, J. Zhang, Y. Zhao, H. Li, H.X. Li, K. Wu, G.Q. Xu, W. Chen, Tuning the metal-support interaction in catalysts for highly efficient methane dry reforming reaction, Appl. Catal. B: Environ. 180 (2016) 511–520.
[8] R.J. Giguere, T.L. Bray, S.M. Duncan, G. Majetich, Application of commercial microwave ovens to organic synthesis, Tetrahedron Lett. 27 (1986) 4945–4948.
[9] T.T.P. Pham, K.S. Ro, L. Chen, D. Mahajan, T.J. Siang, U.P.M. Ashik, J.I. Hayashi, D. Pham Minh, D.-V.N. Vo, Microwave-assisted dry reforming of methane for syngas production: a review, Environ. Chem. Lett. 18 (2020) 1987–2019.
[10] H.M. Nguyen, J. Sunarso, C. Li, G.H. Pham, C. Phan, S. Liu, Microwave-assisted catalytic methane reforming: a review, Appl. Catal. A: Gen. 599 (2020), 117620.
[11] B. Fidalgo, A. Domínguez, J.J. Pis, J.A. Menéndez, Microwave-assisted dry reforming of methane, Int. J. Hydrogen Energy 33 (2008) 4337–4344.
[12] H.M. Nguyen, G.H. Pham, R. Ran, R. Vagnoni, V. Pareek, S. Liu, Dry reforming of methane over Co–Mo/Al_2O_3 catalyst under low microwave power irradiation, Catal. Sci. Technol. 8 (2018) 5315–5324.
[13] K. Su, Y. Wang, K. Hu, X. Fang, J. Yao, Q. Li, J. Yang, Ultralight and high-strength SiC_{nw}@SiC foam with highly efficient microwave absorption and heat insulation properties, ACS Appl. Mater. Interfaces 13 (2021) 22017–22030.
[14] J. Liu, J. Tao, L. Gao, X. He, B. Wei, Y. Gu, Z. Yao, J. Zhou, Morphology-size synergy strategy of SiC@C nanoparticles towards lightweight and efficient microwave absorption, Chem. Eng. J. 433 (2022), 134484.
[15] Z. Zhang, G. Zhao, G. Bi, Y. Guo, J. Xie, Monolithic SiC-foam supported Ni-La_2O_3 composites for dry reforming of methane with enhanced carbon resistance, Fuel Proc. Technol. 212 (2021), 106627.
[16] R. Li, W. Xu, J. Deng, J. Zhou, Coke-REsistant Ni–Co/ZrO_2–CaO-based microwave catalyst for highly effective dry reforming of methane by microwave catalysis, Ind. Eng. Chem. Res. 60 (2021) 17458–17468.
[17] I. de Dios García, A. Stankiewicz, H. Nigar, Syngas production via microwave-assisted dry reforming of methane, Catal. Today 362 (2021) 72–80.
[18] Q. Wei, G. Yang, X. Gao, N. Yamane, P. Zhang, G. Liu, N. Tsubaki, Ni/Silicalite-1 coating being coated on SiC foam: a tailor-made monolith catalyst for syngas production using a combined methane reforming process, Chem. Eng. J. 327 (2017) 465–473.
[19] Z. Zhang, G. Zhao, W. Li, J. Zhong, J. Xie, Key properties of Ni/$CeAlO_3$-Al_2O_3/SiC-foam catalysts for biogas reforming: Enhanced stability and CO_2 activation, Fuel 307 (2022), 121799.
[20] S. Wang, J. Xie, Z. Deng, M. Wu, F. Wang, HCHO oxidation over the δ-MnO_2 catalyst: Enhancing oxidative activities of surface lattice oxygen and surface adsorbed oxygen by weakening Mn-O bond, Fuel 344 (2023), 128141.
[21] P. Hu, S. Dong, X. Li, J. Chen, P. Hu, Flower-like $NiCo_2S_4$ microspheres based on nanosheet self-assembly anchored on 3D biomass-derived carbon for efficient microwave absorption, ACS Sustain. Chem. Eng. 8 (2020) 10230–10241.
[22] S. Tamang, S. Aravindan, 3D numerical modelling of microwave heating of SiC susceptor, Appl. Therm. Eng. 162 (2019), 114250.
[23] Y. Liu, X. Liu, X. E, B. Wang, Z. Jia, Q. Chi, G. Wu, Synthesis of Mn_xO_y@C hybrid composites for optimal electromagnetic wave absorption capacity and wideband absorption, J. Mater. Sci. Technol. 103 (2022) 157–164.
[24] T. Durka, G.D. Stefanidis, T. Van Gerven, A.I. Stankiewicz, Microwave-activated methanol steam reforming for hydrogen production, Int. J. Hydrogen Energy 36 (2011) 12843–12852.
[25] N. Haneishi, S. Tsubaki, M.M. Maitani, E. Suzuki, S. Fujii, Y. Wada, Electromagnetic and heat-transfer simulation of the catalytic dehydrogenation of ethylbenzene under microwave irradiation, Ind. Eng. Chem. Res. 56 (2017) 7685–7692.
[26] J. Xie, S. Wang, K. Zhao, M. Wu, F. Wang, Regulating the Pt–MnO_2 interaction and interface for room temperature formaldehyde oxidation, Inorg. Chem. 62 (2023) 904–915.
[27] S. Wang, J. Xie, M. Wu, F. Wang, Crystal facets engineering of γ-MnO_2 catalysts for remarkable enhancement of formaldehyde removal efficiency, Appl. Surf. Sci. 620 (2023), 156803.
[28] K. Han, S. Xu, Y. Wang, S. Wang, L. Zhao, J. Kambonde, H. Yu, W. Shi, F. Wang, Confining Ni and ceria in silica shell as synergistic multifunctional catalyst for methane dry reforming reaction, J. Power Sources 506 (2021), 230232.
[29] K. Han, Y. Wang, S. Wang, Q. Liu, Z. Deng, F. Wang, Narrowing band gap energy of CeO_2 in (Ni/CeO_2)@SiO_2 catalyst for photothermal methane dry reforming, Chem. Eng. J. 421 (2021), 129989.
[30] H.A.M. van Hal, H.T. Hintzen, Compound formation in the Ce_2O_3-SiO_2 system, J. Alloy. Comp. 179 (1992) 77–85.
[31] B. Wang, G.-q Jin, Y.-y Wang, X.-y Guo, Ni-Sm/SiC catalysts prepared by hydrothermal method for carbon dioxide reforming of methane, J. Fuel Chem. Technol. 44 (2016) 1473–1478.
[32] K. Han, W. Yu, L. Xu, Z. Deng, H. Yu, F. Wang, Reducing carbon deposition and enhancing reaction stability by ceria for methane dry reforming over Ni@SiO_2@CeO_2 catalyst, Fuel 291 (2021), 120182.
[33] S. Wang, W. Yu, S. Xu, K. Han, F. Wang, Ammonia from photothermal N_2 hydrogenation over Ni/TiO_2 catalysts under mild conditions, ACS Sustain. Chem. Eng. 10 (2022) 115–123.
[34] S. Wang, K. Han, Z. Deng, F. Wang, CeO_2 Nanorods Decorated with Pt Nanoparticles as Catalysts for Oxidative Elimination of Formaldehyde, ACS Appl. Nano Mater. 5 (2022) 10036–10046.
[35] F. Pagliuca, P. Luches, S. Valeri, Interfacial interaction between cerium oxide and silicon surfaces, Surf. Sci. 607 (2013) 164–169.
[36] A. Feng, T. Hou, Z. Jia, G. Wu, Synthesis of a hierarchical carbon fiber@cobalt ferrite@manganese dioxide composite and its application as a microwave absorber, RSC Adv. 10 (2020) 10510–10518.
[37] J. Liu, Z. Jia, W. Zhou, X. Liu, C. Zhang, B. Xu, G. Wu, Self-assembled MoS_2/magnetic ferrite $CuFe_2O_4$ nanocomposite for high-efficiency microwave absorption, Chem. Eng. J. 429 (2022), 132253.
[38] P. Yin, G. Wu, Y. Tang, S. Liu, Y. Zhang, G. Bu, J. Dai, Y. Zhao, Y. Liu, Structure regulation in N-doping biconical carbon frame decorated with $CoFe_2O_4$ and (Fe,Ni) for broadband microwave absorption, Chem. Eng. J. 446 (2022), 136975.
[39] P. Liu, S. Gao, X. Liu, Y. Huang, W. He, Y. Li, Rational construction of hierarchical hollow CuS@CoS_2 nanoboxes with heterogeneous interfaces for high-efficiency microwave absorption materials, Comp. Part B: Eng. 192 (2020), 107992.

[40] Z. Jia, M. Kong, B. Yu, Y. Ma, J. Pan, G. Wu, Tunable Co/ZnO/C@MWCNTs based on carbon nanotube-coated MOF with excellent microwave absorption properties, J. Mater. Sci. Technol. 127 (2022) 153–163.
[41] Y. Shi, K. Han, F. Wang, Ni–Cu alloy nanoparticles confined by physical encapsulation with SiO_2 and chemical metal–support interaction with CeO_2 for methane dry reforming, Inorg. Chem. 61 (2022) 15619–15628.
[42] A. Kokel, C. Schäfer, B. Török, Application of microwave-assisted heterogeneous catalysis in sustainable synthesis design, Green Chem. 19 (2017) 3729–3751.
[43] J. Hunt, A. Ferrari, A. Lita, M. Crosswhite, B. Ashley, A.E. Stiegman, Microwave-specific enhancement of the carbon–carbon dioxide (Boudouard) reaction, J. Phys. Chem. C 117 (2013) 26871–26880.
[44] J.K.S. Wan, Microwaves and chemistry: the catalysis of an exciting marriage, Res. Chem. Intermed. 19 (1993) 147–158.
[45] L. Yao, J. Shi, H. Xu, W. Shen, C. Hu, Low-temperature CO_2 reforming of methane on Zr-promoted Ni/SiO_2 catalyst, Fuel Proc. Technol. 144 (2016) 1–7.
[46] S. Wang, A. Comprehensive, Study on carbon dioxide reforming of methane over Ni/γ-Al_2O_3 catalysts, Ind. Eng. Chem. Res. 38 (1999) 2615–2625.
[47] B. Fidalgo, A. Arenillas, J.A. Menéndez, Mixtures of carbon and Ni/Al_2O_3 as catalysts for the microwave-assisted CO_2 reforming of CH_4, Fuel Proc. Technol. 92 (2011) 1531–1536.
[48] C.M. Marin, E.J. Popczun, T.-D. Nguyen-Phan, D.N. Tafen, D. Alfonso, I. Waluyo, A. Hunt, D.R. Kauffman, Designing perovskite catalysts for controlled active-site exsolution in the microwave dry reforming of methane, Appl. Catal. B: Environ. 284 (2021), 119711.
[49] R.L.B.A. Medeiros, G.P. Figueredo, H.P. Macedo, Â.A.S. Oliveira, R.C. Rabelo-Neto, D.M.A. Melo, R.M. Braga, M.A.F. Melo, One-pot microwave-assisted combustion synthesis of Ni-Al2O3 nanocatalysts for hydrogen production via dry reforming of methane, Fuel 287 (2021), 119511.
[50] M. Zhang, Y. Gao, Y. Mao, W. Wang, J. Sun, Z. Song, J. Sun, X. Zhao, Enhanced dry reforming of methane by microwave-mediated confined catalysis over Ni-La/AC catalyst, Chem. Eng. J. 451 (2023), 138616.
[51] M. Kosari, S. Askari, A.M. Seayad, S. Xi, S. Kawi, A. Borgna, H.C. Zeng, Strong coke-resistivity of spherical hollow Ni/SiO_2 catalysts with shell-confined high-content Ni nanoparticles for methane dry reforming with CO_2, Appl. Catal. B: Environ. 310 (2022), 121360.
[52] Y. Song, E. Ozdemir, S. Ramesh, A. Adishev, S. Subramanian, A. Harale, M. Albuali, B.A. Fadhel, A. Jamal, D. Moon, S.H. Choi, C.T. Yavuz, Dry reforming of methane by stable Ni-Mo nanocatalysts on single-crystalline MgO, Science 367 (2020) 777–781.
[53] R. Zhou, M. Mohamedali, Y. Ren, Q. Lu, N. Mahinpey, Facile synthesis of multi-layered nanostructured Ni/CeO_2 catalyst plus in-situ pre-treatment for efficient dry reforming of methane, Appl. Catal. B: Environ. 316 (2022), 121696.
[54] J. Dong, Q. Fu, H. Li, J. Xiao, B. Yang, B. Zhang, Y. Bai, T. Song, R. Zhang, L. Gao, J. Cai, H. Zhang, Z. Liu, X. Bao, Reaction-induced strong metal-support interactions between metals and inert boron nitride nanosheets, J. Am. Chem. Soc. 142 (2020) 17167–17174.
[55] S.W. Jang, S. Dutta, A. Kumar, S.M. Kim, Y.-W. You, I.S. Lee, Silica-enveloped 2D-sheet-to-nanocrystals conversion for resilient catalytic dry reforming of methane, Small 17 (2021) 2102851.
[56] F. Zeng, J. Zhang, R. Xu, R. Zhang, J. Ge, Highly dispersed Ni/MgO-mSiO_2 catalysts with excellent activity and stability for dry reforming of methane, Nano Res. 15 (2022) 5004–5013.
[57] F. Wang, K. Han, L. Xu, H. Yu, W. Shi, Ni/SiO_2 catalyst prepared by strong electrostatic adsorption for a low-temperature methane dry reforming reaction, Ind. Eng. Chem. Res. 60 (2021) 3324–3333.
[58] D. Wang, P. Littlewood, T.J. Marks, P.C. Stair, E. Weitz, Coking can enhance product yields in the dry reforming of methane, ACS Catal. 12 (2022) 8352–8362.
[59] F. Wang, K. Han, W. Yu, L. Zhao, Y. Wang, X. Wang, H. Yu, W. Shi, Low temperature CO_2 reforming with methane reaction over CeO_2-modified Ni@SiO_2 catalysts, ACS Appl. Mater. Interfaces 12 (2020) 35022–35034.